CVS decomposition of 3D homogeneous turbulence using orthogonal wavelets

By **Marie Farge†, Kai Schneider‡, Giulio Pellegrino¶, A. A. Wray|| AND R. S. Rogallo||**

This paper compares the filtering used in Coherent Vortex Simulation (CVS) decomposition with an orthogonal wavelet basis, with the Proper Orthogonal Decomposition (POD) or Fourier filtering. Both methods are applied to a field of DNS data of 3D forced homogeneous isotropic turbulence at microscale Reynolds number $R_\lambda = 168$. We show that, with only $3\%N$ retained modes, CVS filtering separates the coherent vortex tubes from the incoherent background flow. The latter is structureless, has an equipartition energy spectrum, and has a Gaussian velocity probability distribution function (PDF) and an exponential vorticity PDF. On the other hand, the Fourier basis does not extract the coherent vortex tubes cleanly and leaves organized structures in the residual high-wavenumber modes whose PDFs are stretched exponentials for both the velocity and the vorticity.

---

1. Introduction

Since the work presented in this paper has been performed at NASA-Ames, we recall the comments on turbulence research made by Hugh L. Dryden, the first director of NACA (later NASA) (Dryden (1948)).

Dryden begins his paper by saying:

There have been no notable advances in the theory of fully-developed turbulent motion during the last decade. [...] In the period 1934-1938 Taylor developed his statistical theory of turbulence, which was so fruitful in treating the problem of isotropic turbulence. Von Kármán extended the theory, clothed it in more elegant mathematical form, and attempted, with incomplete success, to treat the problem of shear flow. [...] At the Fifth International Congress of Applied Mechanics in 1938 [...] Tollmien and Prandtl suggested that the turbulent fluctuations might consist of two components, one derivable from a harmonic function and the other satisfying an equation of the heat conduction type, i.e. a nondiffusive and a diffusive component or viscosity independent and viscosity dependent type.

Tollmien and Prandtl's suggestion to split the turbulent fluctuations into non-diffusive and diffusive components is very similar to the concept behind CVS which we introduced in Farge, Schneider & Kevlahan (1999). CVS tracks the nonlinear dynamics using an adaptive wavelet basis which captures the regions of strong vorticity gradients at all scales (Schneider Kevlahan & Farge (1997), Schneider & Farge (1998)) and discards the diffusive components which have reached a statistical equilibrium as characterized by

† Laboratoire de Météorologie Dynamique, Ecole Normale Supérieure, Paris, France
‡ Centre de Mathématiques et d'Informatique, Université de Provence, Marseille, France
¶ Institüt für Chemische Technik, Universität Karlsruhe (TH), Germany
|| NASA Ames Research Center, Moffett Field, CA

a Gaussian velocity probability distribution and energy equipartition spectrum (Farge, Schneider & Kevlahan (1999), Farge & Schneider (2000)). This will be shown in this paper.

Later, Dryden affirms that:

The mixing length concept seems wholly inadequate [...], the "mean free path", mixing length, or scale of the turbulent processes is large compared with the thickness of the boundary layer. Considerable masses of fluid move as more or less coherent units. The process cannot be smoothed by averaging over a small volume because it is not possible to choose dimensions small compared with a single fluid element. The mixing length idea, that the turbulent fluctuations and the turbulent shear stress are directly related to the mean speed at a point and its derivatives at that point, must be abandoned. Shall the flow then be regarded as a mean flow that merely transports and distorts large eddies superposed on the flow, these eddies being of varying size and intensity?

This comment of Dryden, stating that the turbulent flows are composed of coherent units of varying size and intensity which cannot be smoothed by averaging, supports our proposal for using the wavelet representation to study turbulent flows (Farge & Rabreau (1988), Farge (1992)). We showed, using the continuous wavelet transform, that coherent vortices in two-dimensional turbulent flows are multiscale eddies with activity covering the entire inertial range. Later on, during the CTR Summer Program 1990, we confirmed that the same is true for three-dimensional turbulent flows and that coherent vortices are responsible for the for flow intermittency (Farge, Guezennec, Ho & Meneveau (1990)).

Finally Dryden concludes by saying that:

The rapidly developing theory of random functions (Bass (1945)) may possibly form the mathematical framework of an improved theory of turbulence. However it is necessary to separate the random processes from the non-random processes. It is not yet fully clear what the random elements are in turbulent flows. The experimental results described suggest that the ideas of Tollmien and Prandtl, that the measured fluctuations include both random and non-random elements, are correct, but as yet there is no known procedure either experimental or theoretical for separating them.

Over the last ten years (Farge (1992), Farge, Goirand, Meyer, Pascal & Wickerhaüser (1992), Farge, Schneider & Kevlahan (1999)), we have developed the filtering process that forms the basis of the CVS method to separate the turbulent fluctuations into organized and random components. It is based on a nonlinear filtering of the vorticity projected on an orthogonal wavelet basis. We derived this procedure using theorems of Donoho and Johnstone, proving optimality of the wavelet representation for denoising signals in the presence of Gaussian white noise, in the sense that wavelet-based estimators minimize the maximum L^2-error for functions with inhomogeneous regularity(Donoho (1993), Donoho & Johnstone (1994)).

In this paper we use CVS filtering to decompose a 3D forced homogeneous isotropic turbulent flow into organized and random components. The microscale Reynolds number is $R_\lambda = 168$ and the simulation has resolution $N = 256^3$.

2. CVS decomposition

We consider the vorticity field $\vec{\omega}(\vec{x}) = \nabla \times \vec{V}$, computed at resolution $N = 2^{3J}$, N being the number of grid points and J the number of octaves in each of the three spatial directions. Each component is developed into an orthogonal wavelet series with largest scale $l_{max} = 2^0$ and smallest scale $l_{min} = 2^{J-1}$ using a 3D multi-resolution analysis

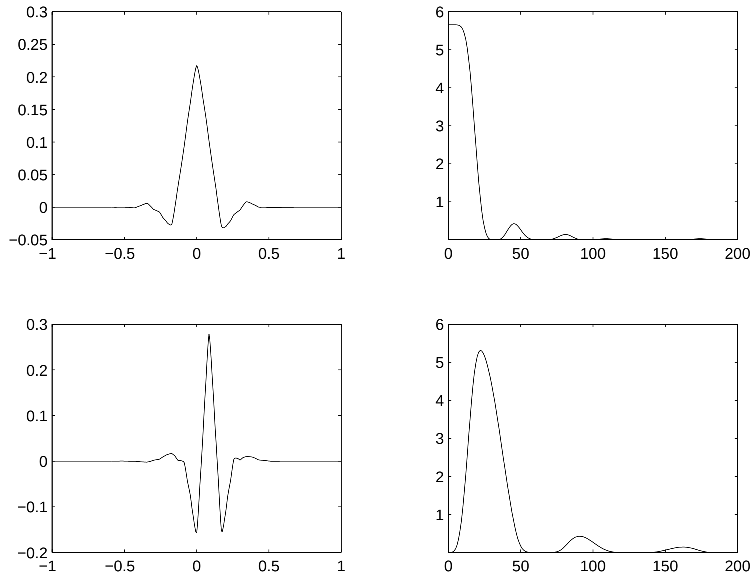

FIGURE 1. Coiflet 12. Top: Scaling function ϕ. Bottom: Corresponding wavelet ψ. (Left: in physical space, right: in Fourier space.)

(MRA) (Daubechies (1992), Farge (1992)):

$$\omega(\vec{x}) \;=\; \bar{\omega}_{0,0,0}\;\phi_{0,0,0}(\vec{x}) \quad + \quad \sum_{j=0}^{J-1}\sum_{i_x=0}^{2^j-1}\sum_{i_y=0}^{2^j-1}\sum_{i_z=0}^{2^j-1}\sum_{\mu=1}^{2^n-1}\;\tilde{\omega}^{\mu}_{j,i_x,i_y,i_z}\;\psi^{\mu}_{j,i_x,i_y,i_z}(\vec{x}) \quad , \tag{2.1}$$

with $\phi_{j,i_x,i_y i,i_z}(\vec{x}) \;=\; \phi_{j,i_x}(x)\;\phi_{j,i_y}(y)\;\phi_{j,i_z}(z)$, and

$$\psi^{\mu}_{j,i_x,i_y,i_z}(\vec{x}) \;=\; \begin{cases} \psi_{j,i_x}(x)\;\phi_{j,i_y}(y)\;\phi_{j,i_z}(z) & ;\; \mu=1 \quad , \\ \phi_{j,i_x}(x)\;\psi_{j,i_y}(y)\;\phi_{j,i_z}(z) & ;\; \mu=2 \quad , \\ \phi_{j,i_x}(x)\;\phi_{j,i_y}(y)\;\psi_{j,i_z}(z) & ;\; \mu=3 \quad , \\ \psi_{j,i_x}(x)\;\phi_{j,i_y}(y)\;\psi_{j,i_z}(z) & ;\; \mu=4 \quad , \\ \psi_{j,i_x}(x)\;\psi_{j,i_y}(y)\;\phi_{j,i_z}(z) & ;\; \mu=5 \quad , \\ \phi_{j,i_x}(x)\;\psi_{j,i_y}(y)\;\psi_{j,i_z}(z) & ;\; \mu=6 \quad , \\ \psi_{j,i_x}(x)\;\psi_{j,i_y}(y)\;\psi_{j,i_z}(z) & ;\; \mu=7 \quad , \end{cases} \tag{2.2}$$

where $\phi_{j,i}$ and $\psi_{j,i}$ are the one-dimensional scaling function (see Fig. 1 top) and the corresponding wavelet (see Fig. 1 bottom), respectively. Due to the orthogonality, the scaling coefficients are given by $\bar{\omega}_{0,0,0} = \langle \omega \, , \, \phi_{0,0,0} \rangle$ and the wavelet coefficients are given by $\tilde{\omega}^{\mu}_{j,i_x,i_y,i_z} = \langle \omega \, , \, \psi^{\mu}_{j,i_x,i_y,i_z} \rangle$, where $\langle \cdot, \cdot \rangle$ denotes the L^2-inner product.

For the orthogonal wavelet basis we use Coiflets 12 (Daubechies (1992)), *i.e.* wavelets with $M = 4$ vanishing moments and a filter length of $3M = 12$ (see Fig. 1 bottom). The advantage of the Coiflets is that they are almost symmetric and that the corresponding scaling functions (see Fig. 1 top) have also M vanishing moments.

We then split the vorticity field into coherent vorticity $\vec{\omega}_C(\vec{x})$ and incoherent vorticity $\vec{\omega}_I(\vec{x})$ by applying nonlinear thresholding to the wavelet coefficients. The choice of the threshold value ϵ is based on theorems derived by Donoho and Johnstone (Donoho (1993), Donoho & Johnstone (1994)) and is $\epsilon = (4/3 Z \log_{10} N)^{1/2}$. Note that ϵ only depends on the total enstrophy Z and the number of grid points N, and there are no adjustable

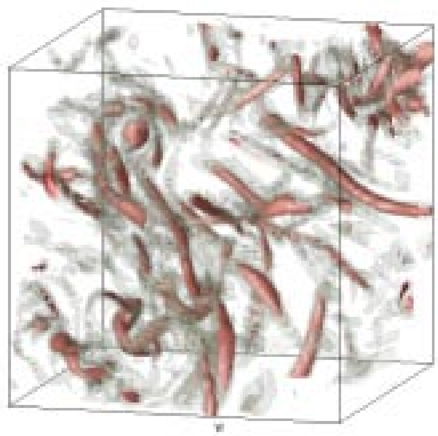

FIGURE 2. Total field: vorticity modulus (isosurfaces $|\vec{\omega}| = 3\sigma, 4\sigma, 5\sigma$, σ being the variance).

parameters. The coherent vorticity field $\vec{\omega}_C$ is reconstructed from the wavelet coefficients whose modulus is larger than ϵ and the incoherent vorticity field $\vec{\omega}_I$ from the wavelet coefficients whose modulus is smaller than or equal to ϵ. The two fields thus obtained, $\vec{\omega}_C$ and $\vec{\omega}_I$, are orthogonal, which ensures separation of the total enstrophy into $Z = Z_C + Z_I$ because the interaction term $\langle \vec{\omega}_C, \vec{\omega}_I \rangle$ vanishes.

Finally we use the Biot-Savart law $\vec{V} = \nabla \times (\nabla^{-2}\vec{\omega})$ to reconstruct the coherent ($\vec{V}_C$) and incoherent $\vec{V}_I$ velocity fields from the corresponding vortices. Since wavelets are almost eigenfunctions of the Biot-Savart kernel (Daubechies (1992)), *i.e.* their localization in both physical and spectral space is well preserved (see Fig. 1), the total energy may be written $E = E_C + E_I - \varepsilon$, with $E = \langle \vec{V}, \vec{V} \rangle$ and $\varepsilon < 0.6\% E$ (see Table I).

The implementation of the CVS decomposition is based on the fast wavelet transform of each vorticity component, thresholding of the coefficients, and the inverse fast wavelet transform for the reconstruction of the coherent and incoherent vortices. The computational cost of the fast wavelet transform is $O(N)$, where N is the number of grid points. The constant of the leading order term corresponds to the filter length $3M$ and depends on the wavelet we use.

3. Application to 3D homogeneous turbulence

We now apply the CVS decomposition to 3D forced homogeneous isotropic turbulence, computed by direct numerical simulation (DNS) at microscale Reynolds number $R_\lambda = 150$ with resolution $N = 256^3$ (for details see Jimenez & Wray (1993)).

In Fig. 2 we plot the modulus of the vorticity fluctuations in the total flow field on a 64^3 subcube. We observe that the field contains well defined vortex tubes, as has been previously observed in laboratory and numerical experiments (Douady, Couder & Brachet (1991), Vincent Meneguzzi (1991)), which are responsible for much of the intermittency of this flow. After decomposing the vorticity field into an orthogonal wavelet series, we calculate the square of each wavelet amplitude, which corresponds to the enstrophy retained in that mode. Subsequently, we sort them by decreasing order of magnitude and compute their partial sum to obtain the compression curve of the wavelet basis. In Fig. 3

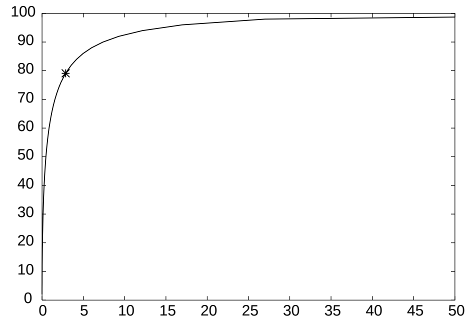

FIGURE 3. Compression curve: % retained enstrophy versus % number of retained wavelets. The star corresponds to the Donoho-Johnstone threshold.

we plot the percentage of retained enstrophy versus the fraction of retained wavelet modes. This curve shows that very few wavelet modes contain most of the enstrophy and that, above 10% of the modes, it saturates rapidly. This saturation corresponds to a quasi-equipartition of the enstrophy, which is characteristic of random fields. In Fig. 3 we indicate by a star the Donoho-Johnstone threshold. This cutoff retains 3% of the wavelet coefficients and 79% of the enstrophy. The coherent vorticity $\vec{\omega}_C$ is then reconstructed from the retained wavelet coefficients, and the incoherent vorticity $\vec{\omega}_I$ is the remainder.

In Table 1 we find that only 3% wavelet modes correspond to the coherent flow, which retains 98.9% of the energy and 79.1% of the enstrophy, while the remaining 97.1% incoherent modes have only 0.5% of the energy and 21% of the enstrophy. The ratio of statistical moments show that the velocity and vorticity skewness is negligible and that this property is preserved by the CVS decomposition. The coherent velocity has the same flatness ($F = 2.9$) as the total velocity, but the incoherent velocity presents a much smaller flatness ($F = 3.4$). The coherent vorticity has a strong flatness ($F = 9.6$) while the incoherent vorticity, likewise, has a reduced flatness ($F = 4.8$).

In Fig. 4 we display the modulus of the coherent (left) and incoherent (right) vorticity fields. Note that the values of the vorticity isosurfaces are the same for the total and the coherent fields while they have been reduced by a factor 2 for the incoherent field since its amplitude is much smaller. In the coherent vorticity (Fig. 4, left) we recognize the same vortex tubes as those present in the total field. In contrast, the incoherent vorticity (Fig. 4, right) is structureless and does not exhibit any organized structures. Hence, the CVS decomposition disentangles the intermittent from the non intermittent contributions, with all the vortex tubes retained in the coherent modes whatever the scale where they are active.

The energy spectra for the total, coherent and incoherent velocity fields, computed using the Biot-Savart law from the corresponding vorticity fields, are plotted in Fig. 5 (left). The spectrum of the coherent contribution is nearly identical to the spectrum of the total flow in the inertial range, i.e. it has $k^{-5/3}$ behavior. Only in the dissipative range does the coherent spectrum decay more rapidly than the incoherent one, since we conjecture that some of the coherent energy is transferred into incoherent energy which is then dissipated. The incoherent contribution exhibits a k^2 scaling which corresponds to energy equipartition. The incoherent velocity field is decorrelated, which makes sense since the incoherent vorticity is structureless (see Fig. 4, right).

To check the dynamical behavior of the coherent and incoherent contributions, we computed their energy transfer in wavenumber space. For practical reasons this has been

quantity	total	coherent	incoherent	large scales	small scales
% of coefficients	100 %	2.9 %	97.1 %	2.9 %	97.1 %
	$\vec{\omega}$	$\vec{\omega}_C$	$\vec{\omega}_I$	$\vec{\omega}_L$	$\vec{\omega}_S$
Enstrophy Z	4895	3872	1024	3455	1440
Enstrophy (percentage)	100 %	79.1 %	20.9 %	70.6 %	29.4 %
Skewness S	-.048	-.056	0.000	-.041	-.002
Flatness F	8.7	9.6	4.8	6.1	9.6
	$\vec{V}$	$\vec{V}_C$	$\vec{V}_I$	$\vec{V}_L$	$\vec{V}_S$
Energy E	43.01	42.56	0.23	42.69	0.33
Energy (percentage)	100.0 %	98.9 %	0.5 %	99.2 %	0.8 %
Skewness S	0.051	0.052	0.000	0.053	0.003
Flatness F	2.9	2.9	3.4	2.8	6.8

TABLE 1. Statistical properties of the vorticity and velocity fields for CVS (left) and POD (right) decompositions.

done at reduced resolution $N = 128^2$. Figure 5 (right) shows that the coherent flow is responsible for most of the energy transfer, giving an energy cascade from large to small scales, and almost vanishes in the viscous range. In contrast, the incoherent flow does not contribute to the energy transfer in the inertial range, but dominates in the dissipative range. From these observations, we put forward the following scenario for the turbulent cascade: the energy injected into the large scales is nonlinearly transferred towards the small scales by nonlinear interactions between the vortex tubes. At the smallest scales, this becomes transfer of coherent energy into incoherent energy which is then dissipated at small scale. We conjecture that, on the contrary, the incoherent background flow does not transfer energy into the coherent flow as it is structureless and well decorrelated. To confirm this we are planning to analyze the nonlinear and the linear terms of 3D Navier-

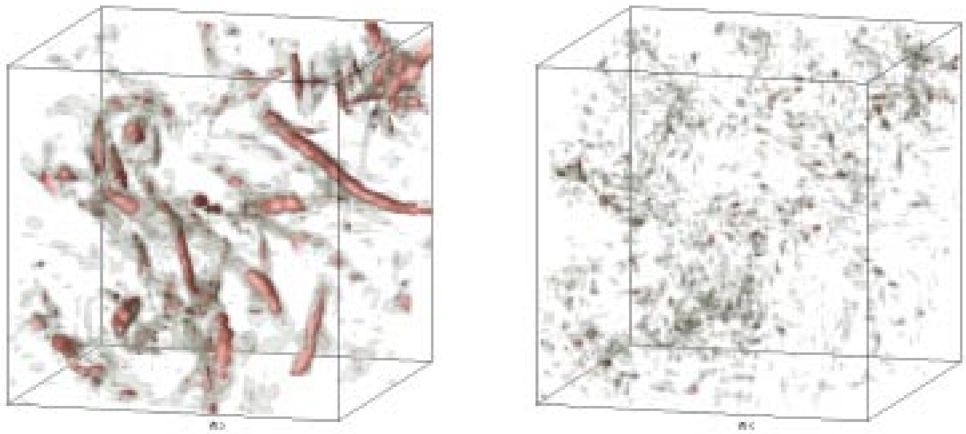

FIGURE 4. CVS decomposition: coherent (left) and incoherent (right) contributions (isosurfaces $|\vec{\omega}| = 3\sigma, 4\sigma, 5\sigma$ and $3/2\sigma, 2\sigma, 5/2\sigma$, respectively).

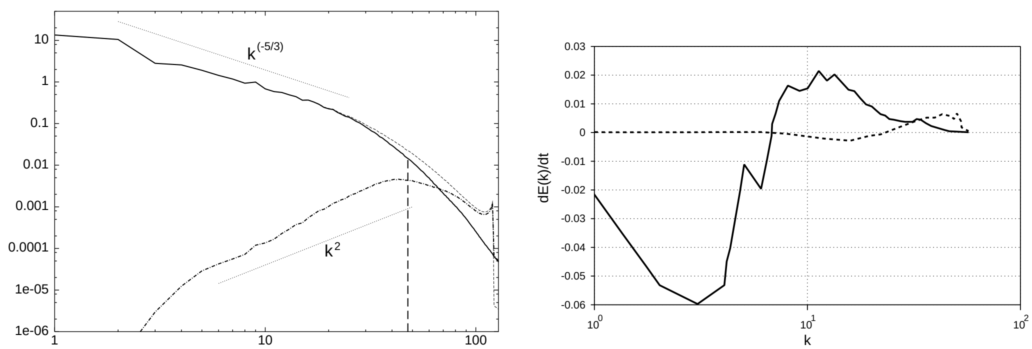

FIGURE 5. Energy spectra $E(k)$,left (Total: ---- ; coherent: ——— ; incoherent: —·— ; Fourier cut: ———) and energy transfers $d_t E(k)$, right (coherent: ——— ; incoherent: ----).

Stokes equations in wavelet space, as we have done for 2D Navier-Stokes equations in the turbulent regime (Schneider & Farge (1998)).

Figure 6 (left) shows the PDF of the velocity in semilogarithmic coordinates. The coherent velocity has the same Gaussian distribution as the total velocity. The PDF of the incoherent velocity is also Gaussian, but its variance is reduced by a factor 13. In contrast to the velocity, the PDF of vorticity (Fig. 7, left) is a stretched exponential with significant tails. The coherent vorticity has the same PDF as the total vorticity including the tails, while the incoherent vorticity has an exponential PDF with much weaker tails.

Since the CVS filtering is based on wavelet denoising and decorrelating without any dynamical assumption or pattern recognition procedure, we now check *a posteriori* that we have actually separated the vortex tubes from the background flow. The coherent vortex tubes can be described as local steady solutions of Euler equations which correspond to regions where there is a depletion of nonlinearity, which happens when the vorticity and velocity vectors are aligned. This situation maximizes the flow helicity $H = \vec{V} \cdot \vec{\omega}$ and corresponds to flow Beltramization (Moffatt H. K. (1985)). To study this tendency towards alignment of the vorticity $\vec{\omega}$ and the velocity $\vec{V}$, we plot in Fig. 8 the PDF of

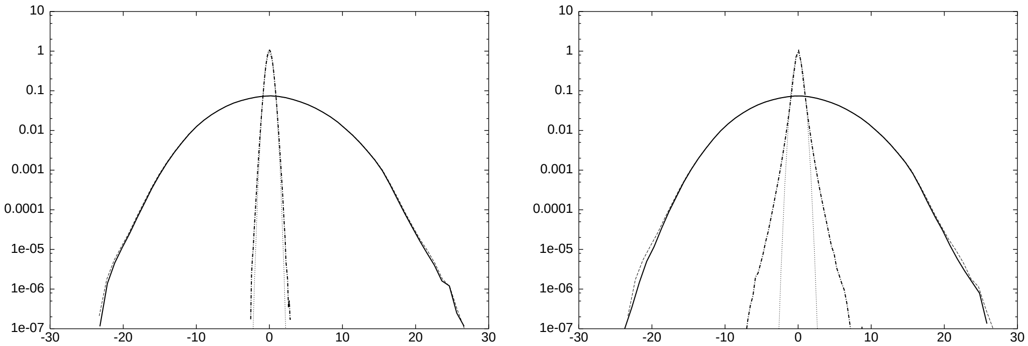

FIGURE 6. PDF of velocity: CVS (left) and POD (right) decompositions. Total: - - - - ; coherent: —— ; incoherent: —·— ; Gaussian fit: ········ .

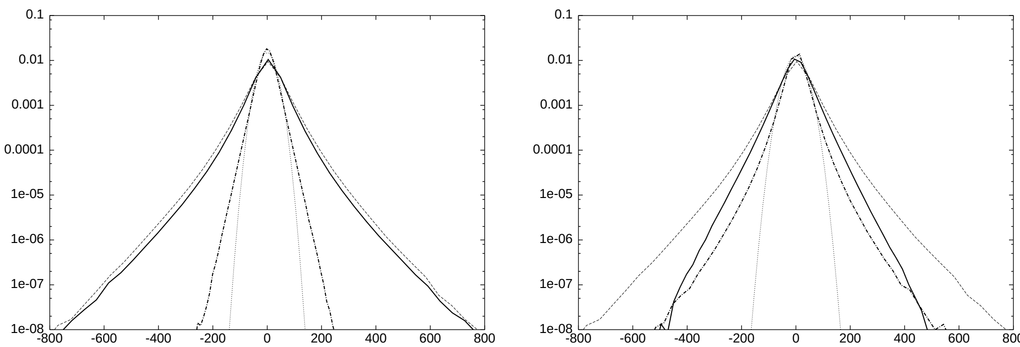

FIGURE 7. PDF of vorticity: CVS (left) and POD (right) decompositions. Total: - - - - ; coherent: —— ; incoherent: —·— ; Gaussian fit: ········ .

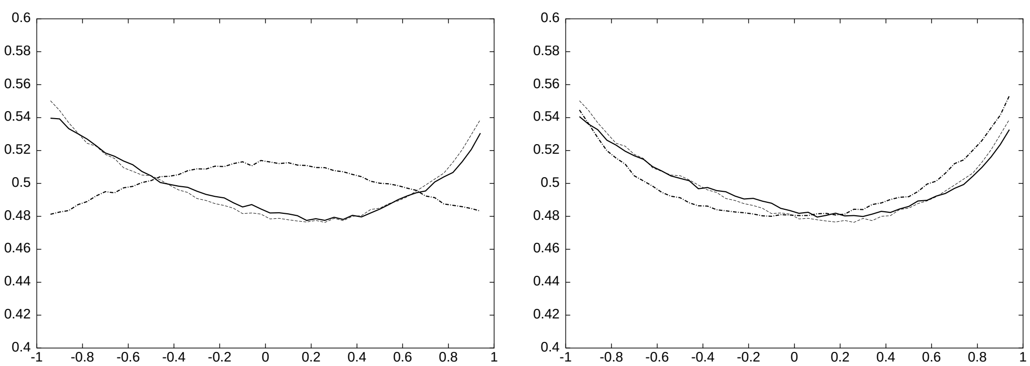

FIGURE 8. PDF of cosine of the angle between velocity and vorticity vectors: CVS (left) and POD (right) decompositions. Total: - - - - ; coherent: —— ; incoherent: —·— .

$\cos\alpha = \frac{\vec{\omega}\cdot\vec{V}}{|\vec{\omega}||\vec{V}|}$. We observe that the coherent contribution has the same tendency towards Beltramization as the total flow, which is characterized by the two maxima encountered in both PDFs for $\alpha = 0^o$ (alignment) and 180^o (anti-alignment). In contrast, the incoherent contribution is more evenly distributed with a maximum at $\alpha = 90^o$, which indicates a tendency towards a local two-dimensionalization since the probability that the vortex stretching term $\vec{\omega}\cdot\nabla\vec{V}$ vanishes is large. This observation, together with the evidence for strong dissipation in the incoherent contribution (see transfers in Fig. 5), agrees with a remark of Moffatt: *Euler flows contain blobs of maximal helicity (positive or negative) which may be interpreted as 'coherent structures', separated by regular surfaces on which vortex sheets, the site of strong viscous dissipation, may be located* (Moffatt H. K. (1985)). Following this picture the coherent vorticity corresponds to the coherent structures, which tend to maximize helicity where vorticity and velocity vectors tend to align with each other, while the incoherent vorticity corresponds to foliated regions which tend to maximize dissipation.

The results discussed here confirm those we obtained for the CVS decomposition of 3D forced homogeneous isotropic turbulent flow computed by DNS at microscale Reynolds number $R_\lambda = 150$ (Vincent Meneguzzi (1991)) with resolution $N = 240^3$ (Farge, Schneider & Pellegrino (2000), Farge & Schneider (2000), Farge, Pellegrino & Schneider (2000)).

4. Divergence problem

Due to the fact that the CVS filtering is nonlinear and the vector valued wavelet basis we have used here (the Coifman 12 wavelet, see Fig. 1) is not divergence-free, *i.e.* $\nabla \cdot \vec{\psi} \neq 0$, the CVS filtering does not yield coherent and incoherent vortices that are divergence-free. We found that, for the case studied here, the divergent contribution of the vorticity field remains below 3% of the total enstrophy. The same problem is also encountered for vortex methods applied to 3D turbulent flows (Winckelmans (1995)). However, the corresponding coherent and incoherent velocity fields are divergence-free since they were reconstructed using the Biot-Savart kernel.

There are several ways to insure that the coherent vorticity remains divergence-free:

- use divergence-free orthogonal wavelets (Lemarié (1992)),
- decompose ω into $\omega = \omega_{div=0} + \nabla\phi$. Then ϕ can be calculated by taking the divergence which leads to a Poisson equation $\nabla^2\phi = \nabla \cdot \omega$,
- apply the previous decomposition, not to the solution, but to the wavelet basis itself, which can be done as a precalculation since the wavelet decomposition is a linear transformation.

We are planning to explore these solutions in future work. It may also be that the divergent contribution of the coherent vorticity field does not significantly affect the flow evolution. To check this we will compare two CVS decompositions for the same flow, one using divergence-free wavelets and the other one using the Coifman 12 wavelet as here, and compute the contribution of the divergent coherent vorticity to the nonlinear terms to see if it remains small.

5. Comparison between CVS and POD decompositions

The procedure CVS decomposition uses to separate turbulent flows into organized and random fluctuations differs from the POD (for details see Berkooz, Holmes & Lumley (1993)). POD, also called Principal Component Analysis (PCA) or Karhunnen-Loève decomposition, computes the auto-correlation tensor of an ensemble of realizations, then diagonalizes it and retains only those eigenmodes corresponding to the $N_>$ largest eigenvalues. This yields the best basis for the ensemble of realizations with respect to the L^2-norm.

In the POD procedure the retained modes are defined *a priori* for all realizations. In contrast, CVS performs the separation *a priori* and selects from a given set of basis functions, the orthogonal wavelets, those having the strongest coefficients. Hence the selection

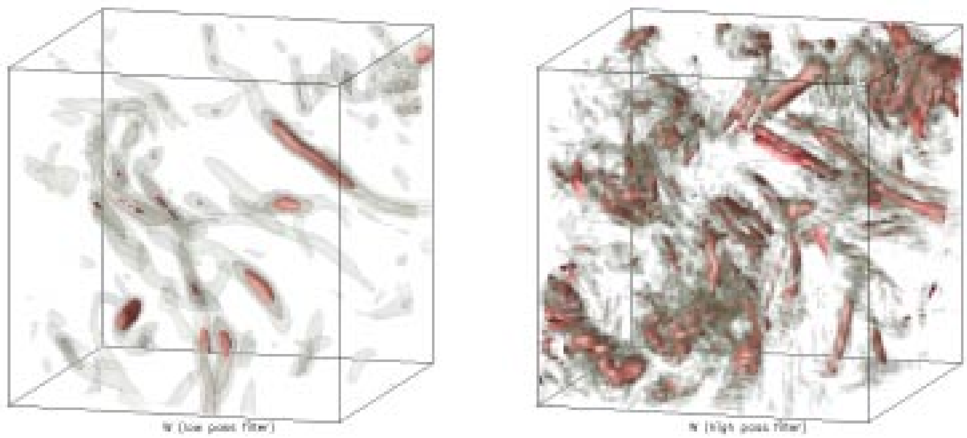

FIGURE 9. POD decomposition: low wavenumber (left) and high wavenumber (right) contributions (isosurfaces $|\vec{\omega}| = 3\sigma, 4\sigma, 5\sigma$ and $3/2\sigma, 2\sigma, 5/2\sigma$, respectively).

procedure is nonlinear, as the retained basis functions depend on the flow realization. From a statistical point of view, the CVS method is based on a Bayesian approach while POD is based on a non-Bayesian (also called frequentist) approach. For the time integration the CVS *a priori* retains the wavelets whose coefficients are larger than the threshold ϵ and some of their neighbors. This selection of the active wavelets is nonlinear because it depends on the direction of the energy and enstrophy transfers in wavelet space which evaluated at the previous time step. Note that the computational cost of POD decomposition scales as N^3, while it scales as N for the CVS decomposition.

For a homogeneous isotropic turbulent flow such as the one studied here, the POD yields the Fourier basis since the correlation tensor is translationally invariant. So we now project the vorticity field on a Fourier basis and split the flow into low and high wavenumber contributions. Note that for this linear separation it doesn't matter whether we decompose the vorticity or the velocity fields, as the Fourier basis diagonalizes the curl operator. To get the same compression ratio as CVS, *i.e.* 3% of the modes retained, the cut-off wavenumber is $k_c = 48$ (see Fig. 5, left). This is a particular case of LES filtering, and the 97% high wavenumber modes are the LES subgrid scale modes.

In Fig. 9 we plot the modulus of vorticity for the POD decomposition. In the low wavenumber modes (left) we observe some vortex tubes. If we compare them with those retained in the CVS coherent vorticity (Fig. 4, left) we find that only a subset of the vortex tubes is extracted and that their structure is smoothed due to the low pass filtering produced by POD in this case. Consequently, the small scale contributions of the vortex tubes are contained in the high wavenumber modes (Fig. 9, right), which exhibit organized structures similar to those found in the total vorticity field (Fig. 2).

Table 1 shows that POD retains 99.2% of the energy, while CVS retains only 98.9%. On the other hand, CVS retains 79.1% of the enstrophy, while POD retains only 70.6%Z. The skewness of velocity and vorticity is negligible, a property preserved by both the CVS and POD decompositions.

In Fig. 7 the vorticity PDFs show that both the large and small scale contributions have strong variance, with the peak of the small scale PDF being slightly larger than that of the large scale PDF. It is important to note that the vorticity PDFs are interchanged compared to the CVS decomposition. The vorticity PDF of the large scales retained by POD is exponential (with flatness 6.1), while it is stretched exponential (with flatness 9.6) for the discarded small scales. The vorticity PDF of the coherent modes retained by CVS is stretched exponential (with flatness 9.6), while it is exponential (with flatness 4.8) for the discarded incoherent vorticity.

Moreover, the velocity PDFs for POD (Fig. 6, right) show that, although the large scale contribution is Gaussian (with flatness 2.9), this is not the case for the small scale contribution which maintains a stretched exponential behavior as for the vorticity PDF (with flatness 6.8). In contrast, the velocity PDFs for CVS (6, left) are Gaussian for both the coherent and the incoherent modes. This non-Gaussian behavior of both the vorticity and velocity PDFs of the POD/LES small scales may make modeling of its effect on the resolved large scales difficult. This difficulty is much less acute with the CVS decomposition since the PDFs of the incoherent contribution is Gaussian for the velocity (6, left) and exponential for the vorticity (7, left).

Concerning the alignment properties between vorticity and velocity, we found that both the large and small scale contributions have the same PDF of $\cos\alpha$ as the total flow (8, right). This is further evidence that coherent vortex tubes are present in both components since, in contrast to CVS, the POD decomposition does not separate different topological behaviors.

6. Conclusion

We have demonstrated that CVS decomposes a 3D forced homogeneous isotropic turbulent flow into organized vortex tubes and a random incoherent background flow. For the same 3D flow, POD, which in this case uses the Fourier basis and is essentially a LES decomposition, does not extract all of the vortex tubes since a lot of organized structures remain in the small scales. Furthermore, the small scales have a stretched exponential probability distribution for both the velocity and the vorticity. In contrast, the incoherent modes of the CVS decomposition have an exponential PDF for the vorticity and a Gaussian distribution for the velocity. Moreover, they are structureless and their energy spectrum shows an energy equipartition, which is not the case for the POD small scales.

In conclusion, we conjecture that modeling of the effect of the discarded modes on the resolved modes may be better justified for CVS than for POD. One should keep in mind that LES of turbulent flows is performed by integrating only one flow realization at a time. The statistics are obtained afterwards by space, time, or ensemble averaging several realizations over time if the flow is statistically steady. Therefore, POD, which is by construction the best basis to represent with a reduced number of modes an ensemble of flow realizations, is not necessarily the best decomposition for computing the flow evolution realization by realization.

We think that the classical strategy of projecting the flow onto a basis and truncating the series to a fixed number of resolved modes can be improved. CVS adopts a nonlinear strategy, which adapts the number of resolved modes to each flow realization, by projecting the flow at each time step onto a wavelet basis, retaining only the strongest wavelet coefficients. In this case all degrees of freedom which contribute to the flow nonlinearity, *i.e.* the coherent modes, are computed whatever their scale, while the remaining degrees of freedom, *i.e.* the incoherent modes, are discarded and modeled, perhaps by a linear dissipation.

The CVS procedure that we have applied to 2D turbulent flows (Farge, Schneider &

Kevlahan (1999)) can be generalized to 3D turbulent flows since we have shown that the incoherent modes are structureless, decorrelated, have an energy equipartition spectrum, and have a Gaussian PDF of the velocity.

A crucial step in the demonstration of the potential of the CVS method is to design an adaptive wavelet solver for the 3D Navier-Stokes equations written in vorticity-velocity formulation, which combines an Eulerian projection of the solution with a Lagrangian procedure for the basis adaption. We have done this for 2D turbulent flows, and we are presently developing it for 3D turbulent flows.

Acknowledgments

M. F. and K. S. thankfully acknowledge financial support from the Center for Turbulence Research, Stanford University. We are very grateful to Joel Ferziger for refereeing and correcting this paper.

REFERENCES

Bass, J. 1945 Les fonctions aléatoires et leur interprétation mécanique. *Revue Sci.* **83**, 3-20.

Berkooz, G., Holmes, P. & Lumley, J. L. 1993, The proper orthogonal decomposition in the analysis of turbulent flows. *Ann. Rev. Fluid Mech.* **25**, 539-575.

Daubechies, I. 1992 *Ten Lectures on wavelets.* SIAM, Philadelphia.

Douady, S., Couder, Y. & Brachet, M. E. 1991 Direct observation of the intermittency of intense vorticity filaments in turbulence. *Phys. Rev. Lett.* **67**, 983-990.

Donoho, D. 1993 Unconditional bases are optimal bases for data compression and statistical estimation. *Appl. Comput. Harmon. Anal.* **1**, 100-115.

Donoho, D. & Johnstone, I. 1994 Ideal spatial adaption via wavelet shrinkage. *Biometrica.* **81**, 425-455.

Dryden, H. L. 1948 Recent advances in the mechanics of boundary layer flow. *Adv. in Applied Mech.* **1**, 1-40.

Farge, M. & Rabreau, G. 1988 Transformée en ondelettes pour détecter et analyser les structures cohérentes dans les écoulements turbulents bidimensionnels. *C. R. Acad. Sci. Paris Série II b.* **307**, 433-440.

Farge, M., Guezennec, Y., Ho, C. M., & Meneveau, C. 1990 Continuous wavelet analysis of coherent structures. *Summer Program Proceedings*, Center for Turbulence Research, NASA Ames/Stanford Univ. 331-343.

Farge, M. 1992 Wavelet Transforms and their Applications to Turbulence. *Ann. Rev. of Fluid Mech.* **24**, 395-457.

Farge, M., Goirand, E., Meyer, Y., Pascal, F. & Wickerhaüser, V. M. 1992 Improved predictability of two-dimensional turbulent flows using wavelet packet compression. *Fluid Dyn. Res.* **10**, 229-345.

Farge, M., Schneider, K., & Kevlahan, N. 1999 Non-Gaussianity and Coherent Vortex Simulation for two-dimensional turbulence using an adaptive orthonormal wavelet basis. *Phys. Fluids.* **11**(8), 2187-2201.

Farge, M. & Schneider, K. 2000 Coherent Vortex Simulation (CVS), a semi-deterministic turbulence model using wavelets. *Flow, Turb. Combust.*, submitted.

Farge, M., Schneider, K. & Pellegrino, G. 2000 Vortex tube extraction in three-dimensional turbulence using orthogonal wavelets. *Advances in Turbulence VIII*, eds. C. Dopazo *et al.*, CIMNE, Barcelona. 797-800.

Farge, M., Pellegrino, G. & Schneider, K. 2000 Coherent vortex extraction in 3D turbulent flows using orthogonal wavelets. *Phys. Rev. Lett.*, submitted.

Jimenez, J. & Wray, A. A. 1993 The structure of intense vorticity in isotropic turbulence. *J. Fluid Mech.* **255**, 65-90.

Lemarié, P. G. 1992 Analyses multirésolutions non orthogonales, commutation entre projecteurs de dérivation et ondelettes à divergence nulle. *Revista Mat. Iberoamericana.* **8**, 221-236.

Moffatt, H. K. 1985 Magnetostatic equilibria and analogous Euler flows of arbitrary complex topology. *J. Fluid Mech.* **150**, 359-378.

Schneider, K., Kevlahan, N. & Farge, M. 1997 Comparison of an adaptive wavelet method and nonlinearly filtered pseudo-spectral methods for two-dimensional turbulence. *Theoret. Comput. Fluid Dyn.* **9**, 191-206.

Schneider, K. & Farge, M. 1997 Wavelet forcing for numerical simulation of two-dimensional turbulence. *C. R. Acad. Sci. Paris, Série II b.* **325**, 263-270.

Schneider, K. & Farge, M. 1998 Wavelet approach for modelling and computing turbulence. *Lecture Series 1998-05 Advances in turbulence modelling*, von Karman Institute for Fluid Dynamics, Bruxelles. 1-132.

Schneider, K. & Farge, M. 2000 Numerical simulation of temporally growing mixing layer in an adaptive wavelet basis. *C. R. Acad. Sci. Paris Série II b.* **328**, 263-269.

Vincent, A. & Meneguzzi, M. 1991 The spatial structure and statistical properties of homogeneous turbulence. *J. Fluid Mech.* **225**, 1-25.

Winckelmans, G. S. 1995 Some progress in large-eddy simulation using the 3D vortex particle method. *Annual Research Briefs*, Center for Turbulence Research, NASA Ames/Stanford Univ. 391-415.